Bend-twist coupling potential of wind turbine blades

Fedorov, Vladimir; Berggreen, Christian

Published in:
Journal of Physics: Conference Series (Online)

Link to article, DOI:
10.1088/1742-6596/524/1/012035

Publication date:
2014

Document Version
Publisher's PDF, also known as Version of record

Bend-twist coupling potential of wind turbine blades

2014 J. Phys.: Conf. Ser. 524 012035

(http://iopscience.iop.org/1742-6596/524/1/012035)

Bend-twist coupling potential of wind turbine blades

V Fedorov[1,3] **and C Berggreen**[2]

[1] Department of Wind Energy, Technical University of Denmark,
Building 114, Frederiksborgvej 399, DK-4000 Roskilde, Denmark
[2] Department of Mechanical Engineering, Technical University of Denmark,
Building 403/026, Nils Koppels Alle, DK-2800 Kgs. Lyngby, Denmark

E-mal: vlfe@dtu.dk

Abstract. In the present study an evaluation of the potential for bend-twist coupling effects in wind turbine blades is addressed. A method for evaluation of the coupling magnitude based on the results of finite element modeling and full-field displacement measurements obtained by experiments is developed and tested on small-scale coupled composite beams. In the proposed method the coupling coefficient for a generic beam is introduced based on the Euler-Bernoulli beam formulation. By applying the developed method for analysis of a commercial wind turbine blade structure it is demonstrated that a bend-twist coupling magnitude of up to 0.2 is feasible to achieve in the baseline blade structure made of glass-fiber reinforced plastics. Further, by substituting the glass-fibers with carbon-fibers the coupling effect can be increased to 0.4. Additionally, the effect of introduction of bend-twist coupling into a blade on such important blade structural properties as bending and torsional stiffness is demonstrated.

1. Introduction

Elastic coupling between bending and torsion in composite beams is fully governed by anisotropy of composite materials. It is naturally done through coupling between in-plane tensile and shear deformations in a generic layer of composite material with the reinforcements, typically fibers, misaligned with the main loading direction. It has been demonstrated that wind-turbine blades with bend-twist coupling (BTC) effects can potentially benefit from the blade coupled response by e.g. achieving significant load mitigation [1, 2].

Presently there is only limited amount of information available in the literature on the BTC magnitudes that are feasible to achieve in modern wind turbine blade structures [3, 4]. It is also of particular interest how introduction of BTC would affect such important blade structural properties as bending stiffness and torsional stiffness.

The main goal of the study is to develop a method for numerical and experimental evaluation of bend-twist coupling effects in generic beams and to apply the developed method to a commercial wind turbine blade structure to investigate coupling magnitudes feasible to achieve in it by simple layup modifications.

The BTC analysis method is presented in this paper first. Then its performance is verified against the results of a beam cross-section analysis tool BECAS. Further, the method is applied to numerical and experimental results for small-scale composite beams and finally BTC magnitudes are calculated for sub-scale components of a commercial wind turbine blade.

[3] To whom any correspondence should be addressed.

2. Method

2.1. Bend-twist coupling in beams

According to the Timoshenko beam formulation, a relation between generalized forces and moments applied to a beam cross-section and the cross-section deformations can be written in form of a 6x6 cross-section stiffness matrix. The formulation accounts for the following beam deformations: Tension, torsion, and transverse shear and bending in two principal directions each. The method proposed here is based on a reduced formulation that relates the cross-section deformations to the generalized loads: Only bending in one principal direction and torsion are accounted for. This basically corresponds to the classical Euler Bernoulli beam formulation which among other things implies rigid cross-sections and no shear deformations.

Thus, for a generic beam cross-section, the relation between generalized loads represented by bending moment M, torque T and beam bending curvature κ_b and rate of twist κ_t can be written in form of a 2x2 compliance matrix:

$$\begin{bmatrix}\kappa_b \\ \kappa_t\end{bmatrix} = \begin{bmatrix}\frac{1}{EI} & S \\ S & \frac{1}{GJ}\end{bmatrix}\begin{bmatrix}M \\ T\end{bmatrix} \tag{1}$$

Following the above formulation, a BTC coefficient β is introduced through the coupling coefficient S, bending stiffness EI and torsional stiffness GJ:

$$\beta = \frac{S}{\frac{1}{EI}\frac{1}{GJ}} = S\sqrt{EIGJ} \tag{2}$$

It can be shown that the BTC coefficient β actually corresponds to the coupling coefficient α introduced by Lobitz [5]. Although, it has to be mentioned that the presently adopted formulation is different since when no BTC exists ($S = 0, \beta = 0$), beam bending response is described in classical form:

$$\kappa_b = \frac{M}{EI} \tag{3}$$

2.2. Bend-twist coupling analysis method

The essence of the method developed for evaluation of coupling coefficient β is in independent application of bending moment and torque to the examined beam configuration (ensuring constant moment distributions along the entire beam length) and analysis of its deformations using the adopted formulation. This can be done numerically using FEM or experimentally using full-field digital image correlation (DIC) measurements. Equation (1) can be resolved by obtaining the beam bending curvatures and twist rates when bending moment is applied to the beam (κ_b^b, κ_t^b), and when torque is applied to the beam (κ_b^t, κ_t^t). Bending and torsional stiffness can be then calculated as:

$$EI = \frac{M}{\kappa_b^b}; \qquad GJ = \frac{T}{\kappa_t^t} \tag{4}$$

Typically the system is over determined and only three beam responses out of four are required to obtain the solution. Therefore the BTC coefficient S can be resolved using either of the two coupled responses:

$$S = \frac{\kappa_t^b}{M} = \frac{\kappa_b^t}{T} \tag{5}$$

2.3. Calculation of beam response

Beam bending (κ_b) and twist (κ_t) deformations can be obtained from a beam FE model of high detail and during experiments using a DIC system. It is typically possible to acquire a 3D displacement field

along the entire beam in both FEM and DIC measurements. By exploiting the fitting algorithm proposed by Arun et. al. in [6], bending displacements and twist angles can be calculated along the beam.

Distributions of bending displacements $w(x)$ and twist angles $\varphi(x)$ along the beam axis X are then represented by polynomials of orders N_w and N_φ accordingly. This is done by least-square fitting into the length-wise bending displacement and twist distributions as follows:

$$w(x) = \sum_{i=0}^{N_w} a_i x^i ; \qquad \varphi(x) = \sum_{i=0}^{N_\varphi} b_i x^i \tag{6}$$

Here a_i and b_i- are coefficients of the fitted polynomials.

According to the Euler-Bernoulli beam formulation, all beam cross-sections remain plain and no shear deformation takes place. Therefore the beam bending curvatures and rates of twist are calculated as:

$$\kappa_b = \frac{d^2 w(x)}{dx^2} = \sum_{i=2}^{N_w} i(i-1) a_i x^{i-2} ; \qquad \kappa_t = \frac{d\varphi(x)}{dx} = \sum_{i=1}^{N_\varphi} i b_i x^{i-1} \tag{7}$$

For higher level of details in the resulting distribution of beam curvatures (e.g. to observe the beam torsional stiffness variation due to constrained warping) it is desirable to use higher polynomial orders N_w and N_φ. However, as the beam curvatures are calculated as derivatives, fluctuations in the final results are expected, especially when they are based on more noisy experimental DIC measurements. Therefore, to improve the quality of the computations it is recommended to provide as dense measurements as possible along the beam length. While this is relatively easy achieved in FEM by refining the mesh, there is often a practical limit for the measurement density when using DIC. Clearly, for equivalent resultant noise levels, the calculations based on FEM results can be done for higher polynomial orders than for those based on DIC measurements.

When selecting the polynomial orders, particular attention should be paid to the end effects occurring as very large values near the ends of the measured region. Those effects are also very sensitive to the selected polynomial orders; this will be shown in more detail in the next section.

Typically, the effect of BTC in the beam response (that is twist under bending or bending under torsion) is considerably lower than the magnitude of the "classical" uncoupled response (bending under bending or twist under torsion). Additionally, taking into account that only one differentiation is needed to obtain twist curvatures, it is reasonable to use the beam twist response under bending κ_t^b in order to get higher quality results for the coupling coefficient S, see equation (5).

2.4. Verification against BECAS

Before the method has been applied to the beam structures of interest, its performance was verified against BECAS [7], a FE tool for analysis of beam cross-sections, operating with full 6x6 Timoshenko beam stiffness matrix formulation and able to predict anisotropy effects. The verification was performed for a case of a prismatic solid beam made of transversely-isotropic material with the fibers biased by 22.5° with respect to the beam axis. The beam geometry is depicted in figure 1 and material properties are given in table 1.

The beam was modeled in ANSYS using 8-node solid finite elements SOLID185 with 20x20 elements along the cross-section and 40 elements along the beam length. The beam was fully clamped at one end and subjected to tip bending moment and torque at the free using master node configuration.

The results for two sets of polynomial orders: N_w= 3 with N_φ= 2 and for N_w= 12 with N_φ= 11 are given in figure 2. It can be seen that the method agrees well with the BECAS results (up to ca. 2-3% error) which indicated that the proposed reduced 2x2 compliance matrix formulation produces rather good results.

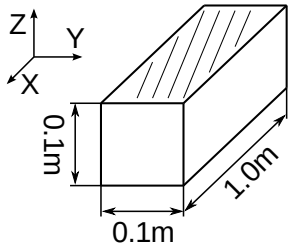

Figure 1. Prismatic beam geometry for verification against BECAS. Fibers are biased by 22.5° with respect to the beam axis.

Table 1. Material properties for prismatic beam used for verification against BECAS.

Parameter	Value
E_{11}	480Pa
$E_{22} = E_{33}$	120 Pa
$G_{12} = G_{13}$	60 Pa
G_{23}	50 Pa
$\nu_{12} = \nu_{13}$	0.19
ν_{23}	0.26

It has to be noted that as seen from the plots in figure 2, the end effects mentioned in the previous section are more pronounced when higher order polynomials are used. Additionally, for this particular case, where the beam response was obtained from a FE model, the polynomial orders as high as 12 did not generate significant noise after differentiation. This is usually not the case when more noisy experimental DIC measurements are processed, therefore, lower orders such as N_w= 3 with N_φ= 2 can be recommended there.

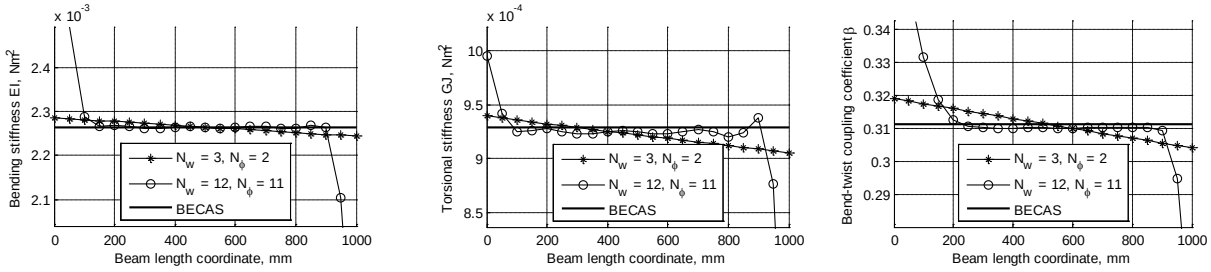

(a) (b) (c)

Figure 2. Variation of bending stiffness EI (a), torsional stiffness GJ (b) and bend-twist coupling coefficient β (c) for clamped solid prismatic beam vs. BECAS results. The plot ranges are limited to ±10% of the BECAS values.

3. Results

3.1. Numerical and experimental results on composite beams

Before being used for analysis of complex structures such as real wind turbine blades, the BTC analysis method was applied to numerical (FEM) and experimental results on small-scale uniform composite beams of simple box- and I-shaped cross-sections. For easier manufacturing, the beams were made from prepreg glass-fiber material and each beam was composed of the following components: Two flanges made from uni-directional (UD) material and two shear webs made of biax (±45°) material, bonded together with epoxy, figure 3. BTC in the beams was introduced by fiber biasing in the UD layers of both flanges: 0°, 15° and 25° to the main beam axis. Hereby, three beam configurations were available for each cross-section type.

Three FE models were developed for each beam configuration. For the reason of performance comparison of different FE model types due to reported issues with shell elements [8, 9], the FE models varied only by the type of finite elements used:

- shell elements;
- shell elements with nodes offset to the beam outer surfaces;
- continuum-shell elements.

The beams were subjected to clamped boundary conditions with a tip bending moment and tip torque applied independently to them. The bending moment applied to all the beams was 0.4 kNm, while the applied torque was 0.2 kNm for box-beams and only of 0.01 kNm for I-beams due to significantly lower torsion stiffness of the I-beams.

The composite beam configurations described above were manufactured and tested using a specially designed test setup based on a four-column testing machine, see figure 4. This complex test setup, originally designed for implementing more advanced loading conditions, was used for application of tip bending moment and tip torque at the beam free end by mean of a pair of equivalent forces applied by compact hydraulic actuators through load clamps mounted on the beams.

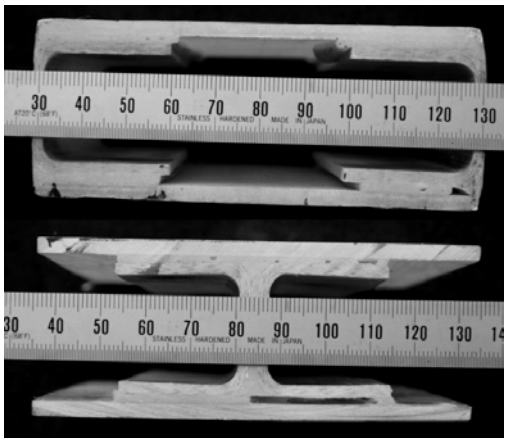

Figure 3. Box- (upper) and I- (lower) cross-sections of the composite beam test specimens.

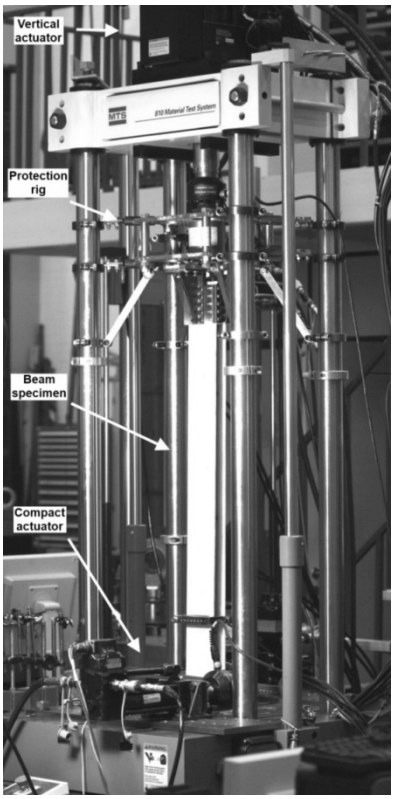

Figure 4. Test setup built around a four-column testing machine for experiments on composite beams.

Polynomial orders of N_w = 3 and N_φ = 2 were adopted as the best with respect to the detail level-to-noise ratio for processing the results of all FE models and experimental measurements. For easier comparison, the final results are presented in form of variations of bending stiffness, torsional stiffness and BTC coefficient along the beams in four groups of plots, see figures 5-8.

The results obtained from FEM and experiments on box-beams are given in figures 5 and 6 accordingly, while similar results for the I-beams are given in figures 7 and 8. Two specimens were tested for each box-beam configuration, while for each I-beam configuration only one specimen was available for testing.

Significant deviations occurred in the results of the box-beam FE models with shell elements where nodes were offset to the outer surface, see figure 5(b). This problem has been reported [8, 9] and hereby the inaccuracy of this type is clearly demonstrated in terms of deviation of torsional stiffness as

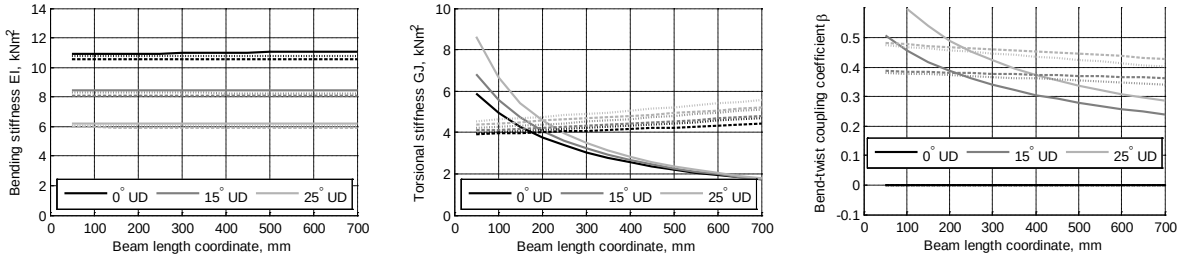

(a) (b) (c)

Figure 5. Results for box-beams based on FEM. A – bending stiffness, b – torsional stiffness, c – BTC coefficient. Results for FE with shell elements and nodal offsets are in solid lines, shell elements without nodal offsets – in dashed lines, continuum-shell elements – in dotted lines.

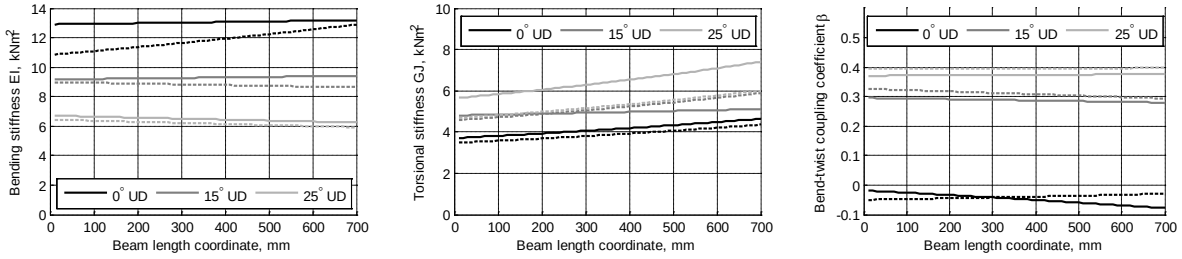

(a) (b) (c)

Figure 6. Results for box-beams based on experimental DIC measurements. A – bending stiffness, b – torsional stiffness, c – BTC coefficient.

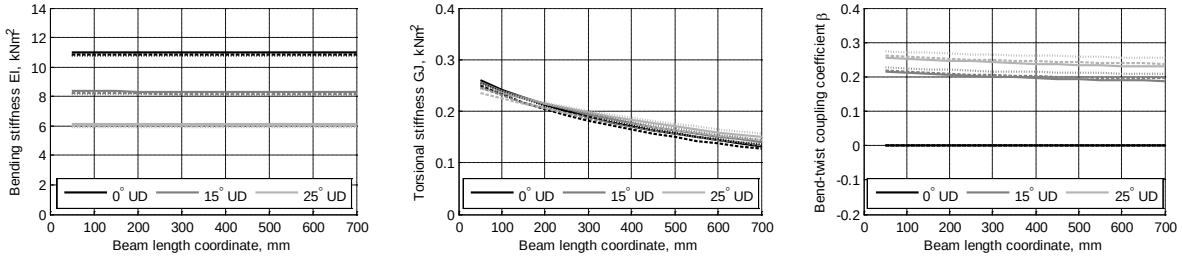

(a) (b) (c)

Figure 7. Results for I-beams based on FEM. A – bending stiffness, b – torsional stiffness, c – BTC coefficient. Results for FE with shell elements and nodal offsets are in solid lines, shell elements without nodal offsets – in dashed lines, continuum-shell elements – in dotted lines.

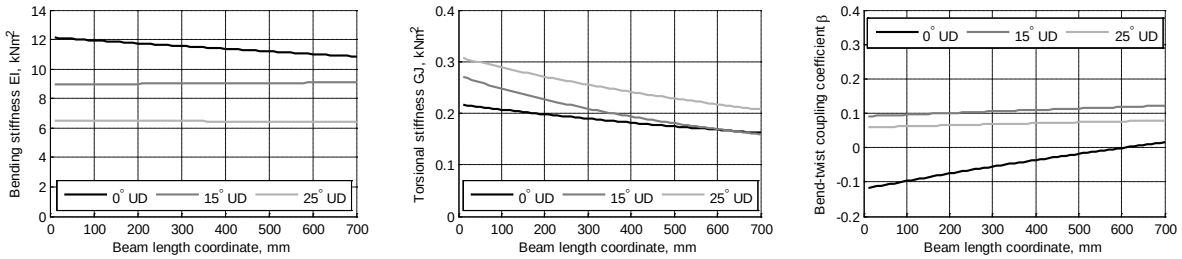

(a) (b) (c)

Figure 8. Results for I-beams based on experimental DIC measurements. A – bending stiffness, b – torsional stiffness, c – BTC coefficient.

well as subsequent BTC coefficient deviation, figure 5(c). However, as seen from figure 7(b), for open cross-sections this problem does not seem to occur.

BTC coefficients obtained for box-beams from the FE models and from the experiments are somewhat different, figures 5(c) and 6(c), with experimental coefficient (0.3-0.4) being slightly lower than the numerical values (0.4-0.5). The same effect but more pronounced is found for the I-beams, see figures 7(c) and 8(c), where the coupling coefficient differs significantly (0.1 vs. 0.2-0.3). It was later realized that the source of the difference was a parasitic torque generated by the reaction forces from the compact actuators when bending moment was applied to the specimens.

The actuators were fixed to the testing machine foundation and in spite of using spherical joints and decoupling elements in the actuator-load clamp connection they still produced parasitic torque which had highest effect on the I-beams owing to low torsional stiffness.

An interesting fact that can be clearly seen from figures 7(b) and 8(b) is a sensitivity of the I-beam torsional stiffness to the clamped boundary conditions due to restricted warping, as reported in [10]. In contrast, from figures 5(b) and 6(b) it is seen that the box-beams are more sensitive to the constraints generated by load clamps. Clearly, both numerical and experimental results agree on these effects.

Apart from the issues highlighted above, the FE results generally agree rather well with the experiments, although some slight deviations can be noticed. Keeping in mind the problem with parasitic torque, the maximum obtained coupling can be estimated as up to 0.35-0.45 for the 25° UD box-beams and up to 0.2-0.3 for the 25° UD I-beams.

3.2. Numerical results on sub-scale components of a commercial blade section

The developed BTC analysis method was applied to the results of FE models of sub-scale components based on a commercial wind turbine blade section [11]. The goal of the study was to investigate possible limits of bend-twist coupling effects in a real blade structure.

The blade section is an 8.4m section of a 23m long wind turbine blade. The blade is built as a load carrying box-spar and the outer shell providing the blade airfoil. The main material used in the blade structure is glass-fiber reinforced plastics (GFRP) with predominantly UD layers in the load carrying spar flanges and biax (±45°) and triax (-45°/0°/+45°) materials prevailing in the other areas including shear webs and sandwich structures. Blade section geometry is depicted in figure 9.

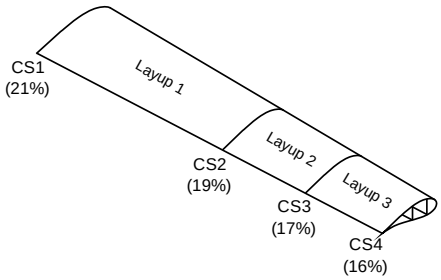

Figure 9. Wind turbine blade section with designated layups, cross-sections and their relative airfoil thicknesses.

Four sub-scale components were selected based on the original blade configuration to study the coupling effects in the blade structure. The sub-scale components are basically 10m long beams of constant cross-sections. Four cross-sections with relative airfoil thicknesses of 16%, 17%, 19% and 21% were selected along the blade section as basis for the sub-scale components, see figures 9 and 10. Significant length of 10m was chosen intentionally, to reduce the unwanted end effects when the BTC analysis method is used.

BTC was introduced to the sub-scale components by varying the fiber directions in the UD layers of the spar flanges. Further, due to the known effect of bending stiffness decrease when fibers are biased from the beam main axis, GFRP material of the UD layers in the spar flanges was substituted by carbon-fiber reinforced plastics (CFRP) to balance the bending stiffness decrease.

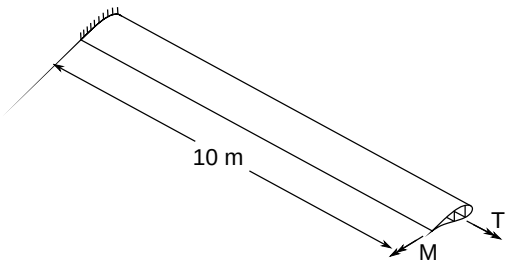

Figure 10. Geometry and boundary conditions for sub-scale components.

FE models with shell elements with no nodal offsets were developed by the author for each of the sub-scale component configuration, see figure 11. Polynomial orders of N_w = 40 and N_φ = 39 were used for the developed BTC analysis method. Mechanical properties of the GFRP and CFRP materials used in the blade spar flanges UD layers are presented in table 2.

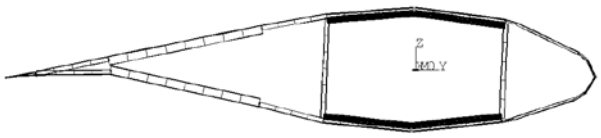

Figure 11. FE modeling of sub-scale component cross-section. Shell elements without nodal offsets are used.

The effect of significant length of the sub-scale components can be seen in figure 12, where calculated distribution of the bending stiffness is presented. The end effects are clearly seen in the plot together with a pronounced plateau (from position 3m to 7m) of constant stiffness value. Similar pattern was found for the distributions of torsional stiffness and bend-twist coupling coefficient. That is the average plateau value that was used for evaluation of each sub-scale component bending and torsional stiffness together with BTC coefficient.

Table 2. Properties of glass-fiber (GFRP) and carbon-fiber (CFRP) reinforced plastics.

Parameter	GFRP	CFRP
E_{11}	39.9 GPa	105 GPa
E_{22}	11.6 GPa	6.82 GPa
G_{12}	4.44 GPa	3.32 GPa
ν_{12}	0.303	0.280

The results for modification of the original GFRP configurations of the sub-scale components are presented in Fig. 13 as variations of bending and torsional stiffness and BTC coefficient with respect to the fiber directions in the UD layers of the blade spar flanges. First note the symmetrical patterns of the variations, which mean that most of the characteristics are in these cases defined by the load carrying spar. Next, note that thinner airfoils are less prone to the bending stiffness variation and more prone to the torsional stiffness variations due to changes in the UD fiber direction. Maximum of the bend-twist coupling coefficient is found to be of ca. 0.2 for the fibers biased 20-25° off the blade main axis. However, bending stiffness in this case is significantly decreased by 30-35%.

The results for modification of the CFRP configurations of the blade sections are presented in figure 14 in a similar fashion as in figure 13 but it is important to note that all the variations are given with respect to the baseline GFRP configurations. Therefore, when no fibers are biased the bending stiffness is ca. 130% higher due to much higher stiffness of the carbon fibers, figure 14(a) and torsional stiffness is ca. 5% lower, figure 14(b), due lower shear stiffness of the CFRP, see table 2.

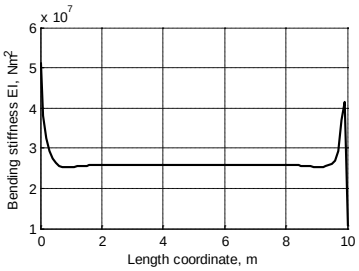

Figure 12. End-effects and plateau in the sub-scale component results. Bending stiffness distribution is taken as an example here. Similar patterns were observed for torsional stiffness and BTC coefficient for all configurations.

For the CFRP configurations the patterns are still found to be symmetric with respect to the fiber biasing but significant increase is achieved in BTC coefficient, see figure 14(c). Slightly higher sensitivity of thinner airfoils to the BTC coefficient is also noticeable there. Maximum of the bend-twist coupling coefficient for the CFRP configurations is found to be of ca. 0.4 when the fibers are biased by the same 20-25°. Bending stiffness is kept nearly the same as in the original GFRP configurations with no fiber biasing.

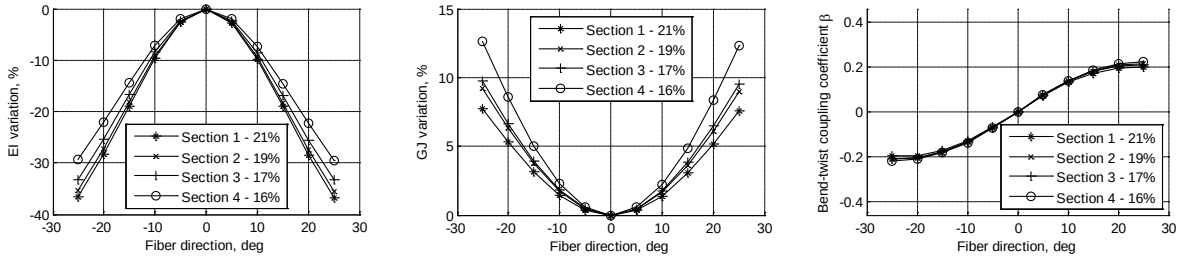

(a) (b) (c)

Figure 13. Effect of the BTC introduction in the original GFRP configuration of the sub-scale components. The results are presented with respect to the baseline configurations with no BTC.

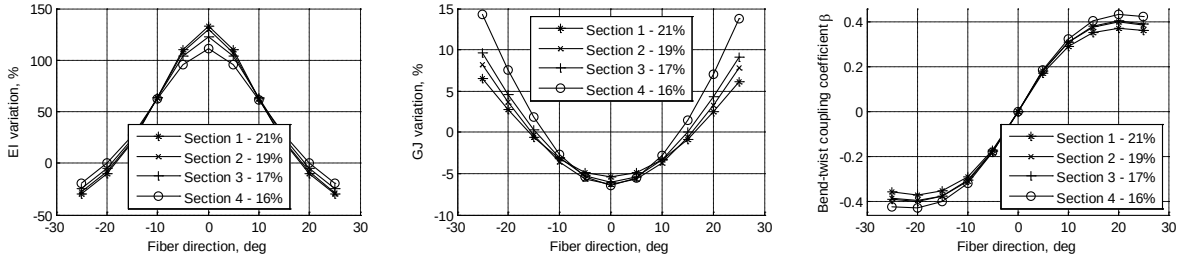

(a) (b) (c)

Figure 14. Effect of the BTC introduction in the configuration of the sub-scale components with GFRP UD material substituted by CFRP. The results are presented with respect to the baseline GFRP configurations with no BTC.

4. Conclusions and future work

A rather efficient and easy to use method for numerical and experimental analysis of BTC effects in beam structures has been developed. It has been demonstrated that by using reduced Euler-Bernoulli compliance matrix formulation it is possible to achieve quite accurate values for the beam stiffness characteristics, very close to those predicted by advanced finite-element codes for beam cross-section analysis such as BECAS. The main advantage of the method is its applicability to both results of FE models and experimental results when DIC measurements on the beam are performed. Another advantage is the capability to capture the effects of constrained warping expressed in variations of the beam stiffness properties along the beam length. It has been demonstrated that the developed method performs well when applied to simple beams and further when applied to analysis of wind turbine blade sub-scale components.

It has been demonstrated that a commercial wind turbine blade structure can achieve maximal BTC coefficient of 0.2 when all the UD fibers in the spar flanges are biased by 20-25°. However, in this case bending stiffness is significantly reduced, by 30-35%. By substituting GFRP by CFRP in the spar UD layers it is possible to achieve BTC coefficient of up to 0.4 and at the same time to preserve the original blade bending stiffness. Thinner airfoils are found to be less sensitive in terms of bending stiffness to the UD fiber biasing, and more sensitive in terms of torsional stiffness. Variations of the BTC coefficients for blades of different airfoil thicknesses are found to be very similar.

The developed bend-twist coupling analysis method is believed to be expandable so that it could account for beam bending stiffness in the second principle direction, and probably beam extension and/or shear characteristics as well. However, incorporating this seems to be a challenging task as more advanced measurement techniques and processing methods might have to be developed.

5. Acknowledgments

Vestas Wind Systems A/S is gratefully acknowledged for providing the wind turbine blade section for the study. The work is partly supported by the Danish Energy Authority through the 2007 Energy Research Programme (EFP 2007). The supported EFP-project is titled “Anisotropic beam model for analysis and design of passive controlled wind turbine blades” and has journal no. 33033-0075.

References

[1] Lobitz D W, Veers P S and Migliore P G 1996 Enhanced performance of HAWTs using adaptive blades *Proceedings of the Wind Energy 96, ASME Wind Energy Symposium, Jan. 29- Feb. 2, 1996, Houston* http://www.aiaa.org

[2] Berry D and Ashwill T 2007 Design of 9-meter carbon-fiberglass prototype blades: CX-100 and TX-100 *Technical Report SAND2007-0201* Sandia National Laboratories, Albuquerque, NM

[3] Bottasso C L, Campagnolo F, Croce A and Tibaldi C 2013 Optimization-based study of bend-twist coupled rotor blades for passive and integrated passive/active load alleviation *Wind Energy* **16** 1149-66

[4] Taeseong K, Hansen A M and Branner K 2013 Development of an anisotropic beam finite element for composite wind turbine blades in multibody system *Renewable Energy* **59** 172-183

[5] Lobitz D and Veers P 1998 Aeroelastic behavior of twist-coupled HAWT blades *Proceedings of the AIAA/ASME Wind Energy Symposium, Reno, Nevada* http://www.aiaa.org

[6] Arun K S, Huang T S and Blostein S D 1987 Least-squares fitting of two 3-D point sets *IEEE Transactions on Pattern Analysis and Machine Intelligence* **9** 698-700

[7] Blasques J P and Stolpe M 2012 Multi-material topology optimization of laminated composite beam cross sections *Composite Structures* **94** 3278-89

[8] Laird D L, Montoya F C and Malcolm D J 2005 Finite element modeling of wind turbine blades *Proceedings of the AIAA/ASME Wind Energy Symposium, Reno, Nevada* http://www.aiaa.org

[9] Fedorov V, Dimitrov N, Berggreen C, Krenk S, Branner K and Berring P 2009 Investigation of structural behavior due to bend-twist couplings in wind turbine blades *Proceedings of the 17th International Conference of Composite Materials (ICCM), Edinburgh, UK* http://www.iccm-central.org/Conferences.html

[10] Chandra R and Chopra I 1992 Structural response of composite beams and blades with elastic couplings *Composite Engineering* **2(5-7)** 347-374

[11] Berring P, Branner K, Berggreen C and Knudsen H 2007 Torsional performance of wind turbine blades part I: Experimental investigation *Proceedings of the 16th International Conference on Composite Materials, ICCM-16 – “A Giant Step Towards Environmental Awareness: From Green Composites to Aerospace”, Kyoto, Japan* http://www.iccm-central.org/Conferences.html